C103-E157

SHIMADZU
Excellence in Science

FTIR TALK LETTER

Vol. 46

It's the season when the green maple leaves are at their most beautiful.
The vivid red of traditional Japanese umbrellas lends an air of elegance.

Microplastics: Human Health Impacts and Current Research



Department of Surgical Oncology, Nagasaki University School of Medicine
Keitaro Matsumoto, Mariko Yamashita, Tomohiro Obata

1. Microplastics

In addition to the direct damage that plastic waste causes to marine ecosystems, concern is growing worldwide about its indirect effects on human health through pathways such as the food chain. Marine plastic pollution is particularly severe in Asia. In Japan, public awareness has increased substantially, leading to initiatives such as restrictions on plastic shopping bags and efforts to reduce plastic production, improve waste collection, and enhance recycling. Plastics degrade and fragment when exposed to ultraviolet radiation from sunlight and physical forces such as ocean waves, generating microplastics and nanoplastics (Fig. 1). (In this article they are collectively referred to as MPs.)

MPs are classified into two categories: primary and secondary. Primary MPs are plastics intentionally produced in sizes smaller than 5 mm (such as the microbeads used in facial cleansers and cosmetic products). Secondary MPs include fragments resulting from the breakdown of plastic products released into the environment due to physical forces, such as ultraviolet light and heat, as well as fibers shed from synthetic clothing during washing. MPs generally refer to plastic particles measuring 5 mm or less. In recent years, concerns have progressed beyond marine pollution to include inhalation exposure, that is, exposure through inhalation of airborne particles. In particular, particles measuring less than several tens of micrometers—and especially those ranging from several micrometers to sub-micrometer sizes—are suspected to be strongly associated with respiratory diseases, as they can settle in the upper respiratory tract as well as in the peripheral lung and alveolar regions.

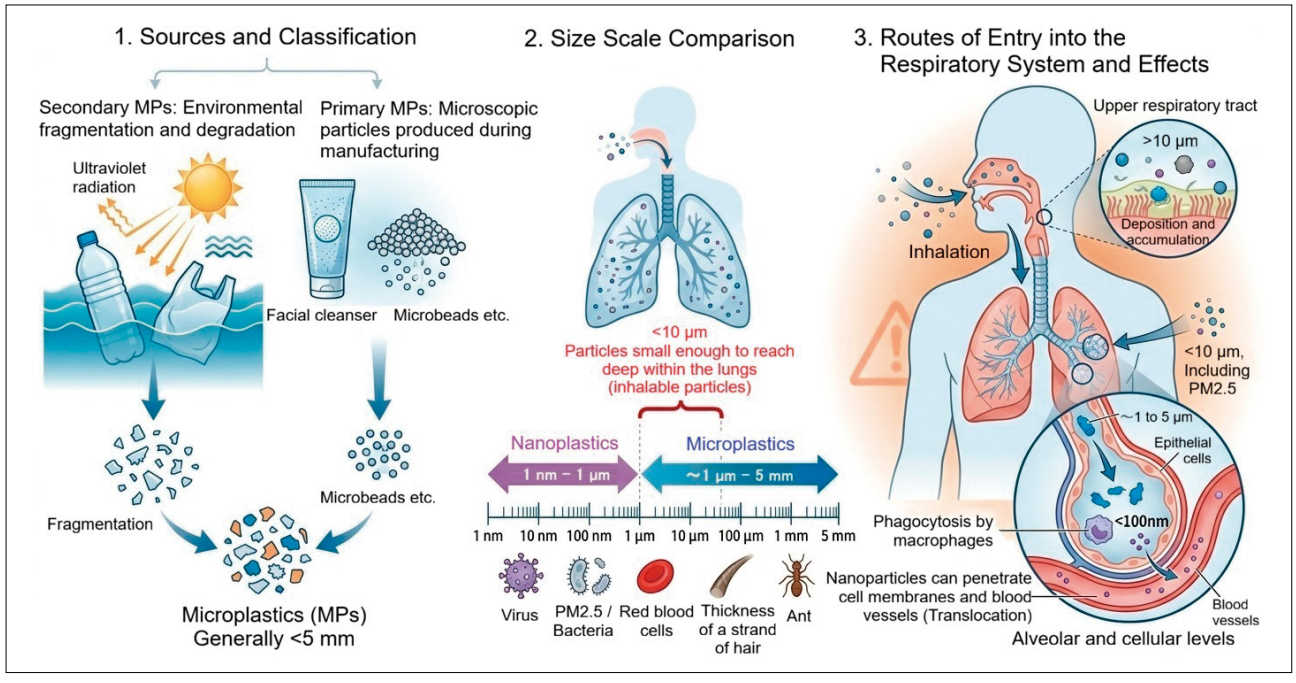

Fig. 1 Sources of Microplastics, Size Classification, and Effects on the Respiratory System

2. Microplastics and Respiratory Disease

Two major categories of respiratory disease have emerged as key areas of interest.

(1) Inflammatory Lung Diseases

The first category includes inflammatory lung diseases (COPD, asthma, chronic airway inflammation, and interstitial lung disease). Since MPs act as particulate irritants, causing epithelial damage, eliciting a macrophage response, inducing inflammatory cytokines (such as IL-6), and amplifying oxidative stress, they may exacerbate existing conditions. MPs may be associated with respiratory disease primarily through oxidative stress and inflammation.

(2) Lung Cancer

The second area of concern is lung cancer. At present, epidemiological evidence is insufficient to establish a causal link between MPs and lung cancer. However, chronic inflammation, oxidative stress, and a fibrotic microenvironment may allow MPs to act as a tumor promoter. Because the lung is continuously exposed to the external environment and environmental pollutants such as PM2.5 are already known risk factors for lung cancer, MPs are increasingly being investigated as potential environmental modifiers of cancer risk.

Advances in Research

Research on microplastics began with (1) assessing their abundance in the environment (seawater, soil, and the atmosphere), but since the 2020s, it has rapidly expanded to include (2) detection in the human body (blood, placenta, lungs, etc.), (3) toxicology (inflammation, fibrosis, and immune dysfunction), and (4) links to disease (epidemiology and clinical studies). In the field of respiratory medicine, in particular, reports of MP detection in human lung tissue have attracted significant attention; Jenner et al. identified MPs using μFTIR, thereby demonstrating the inhalation-to-lung deposition pathway (although the detection limit was approximately 3 μm). More recently, researchers have combined multiple analytical techniques—including Raman microscopy, μFTIR, and pyrolysis GC–MS (Py-GC-MS)—to achieve both qualitative and quantitative analysis of MPs in biological samples. Studies using animal models have reported that pulmonary fibrosis, mediated by oxidative stress and Wnt/β-catenin activation, occurs following intratracheal administration of common polymers such as polystyrene (PS), and studies investigating the underlying molecular mechanisms are ongoing.

3. Technical Challenges in Detecting Microplastics in Biological Tissues

A major obstacle to understanding the biological effects of MPs is the difficulty of detecting and identifying them in biological samples. Current analytical methods include fluorescent staining techniques, such as Nile Red staining, Fourier-transform infrared (FTIR) spectroscopy, and Raman spectroscopy. However, several important challenges remain.

(1) False Positives

Nile Red staining is simple and widely used, but it also reacts with biological lipids and other organic materials. Consequently, distinguishing MPs from endogenous tissue components can be difficult (Fig. 2).

(2) Inefficient Particle Search

Although micro-Raman spectroscopy is excellent for the chemical identification of polymers, locating micrometer-sized particles within large lung tissue sections is extremely time-consuming, making the method poorly suited for routine screening of clinical samples.

(3) Loss During Tissue Processing

Conventional pathological specimen preparation frequently results in the loss of hydrophobic MPs from tissue samples.

Establishing a method to accurately identify the location and types of MPs within the lungs—by overcoming these technical challenges—will be the first step toward elucidating the underlying pathology. Rigorous contamination control and blank-sample management are also critical.

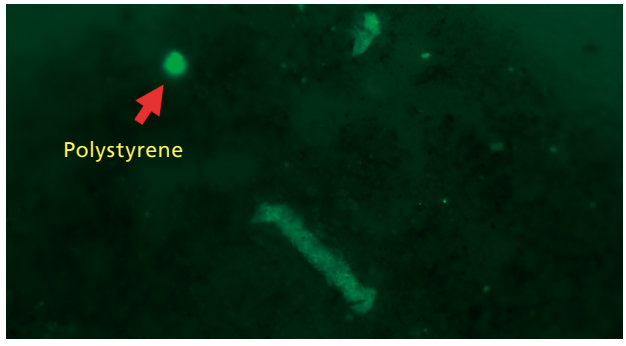

Fig. 2 Identification of Microplastics by Nile Red Staining and Fluorescence Microscopy

4. Research Approach at Nagasaki University

Our research group in the Department of Surgical Oncology at Nagasaki University is addressing these challenges through a multidisciplinary approach in collaboration with the Department of Respiratory Medicine and the Nagafuchi Laboratory at Fukuoka Institute of Technology. The project combines analyses of human clinical specimens with animal studies using mouse models.

(1) Detection of MPs in Human Lung Samples

Our group has been conducting analyses using surplus specimens obtained from lung cancer resections and bronchoalveolar lavage (BAL) fluid collected during clinical procedures. In joint research with Fukuoka Institute of Technology, we successfully detected MPs—including polystyrene (PS), polypropylene (PP), and polyethylene (PE)—in human lung tissue using micro-Raman spectroscopy (1). That research provided direct evidence that airborne MPs can reach and accumulate in the deep lung, and serves as the foundation of our research program. Like other studies, the work demonstrates sufficient evidence of an association between microplastic levels and disease. However, the challenges mentioned earlier remain.

(2) Issues and Solutions in Mouse MP Exposure Experiments

To verify phenomena observed in humans and gain insight into the underlying disease mechanisms, we are conducting experiments involving the intratracheal administration of MPs in mice. In our initial studies, non-fluorescent polystyrene beads (3 μm and 6 μm in diameter) were administered intratracheally, and conventional pathological specimens were prepared using formalin fixation and paraffin embedding (FFPE). However, when the specimens stained with hematoxylin and eosin (HE) were examined under a microscope, a problem was observed: the MPs that should have been present in the tissue were absent.

Further investigation showed that the hydrophobic polystyrene particles had either dissolved or detached from the tissue during paraffin embedding and staining due to exposure to organic solvents such as xylene and alcohol. Consequently, only spherical voids remained at the former particle locations, preventing direct assessment of the interactions between the MPs and surrounding cells. These findings highlight the limitations of applying conventional pathological methods directly to MP research.

- **Solution 1: Fluorescently Labeled MPs and Frozen Sections**

To avoid the dehydration and lipid-removal steps associated with paraffin embedding, we switched to preparing frozen sections from unfixed or briefly fixed lung tissue. To improve visualization, fluorescent dye-labeled polystyrene particles were used. By combining fluorescent particle imaging with DAPI nuclear staining, we successfully visualized the localization of MPs within the airway and alveolar regions using fluorescence microscopy (Fig. 3).

- **Solution 2: Establishing Endotracheal Administration Techniques**

In early experiments, it was sometimes unclear whether the MPs reached the deep regions of the lungs. We therefore established a method for administering the MPs under endotracheal intubation using a laryngoscope and a guidewire. This method enabled reliable delivery of MP suspensions into the trachea via a Surflo needle, resulting in uniform distribution throughout the lungs. In fact, macroscopic examination of mouse lungs using this method has confirmed that the fluorescent beads are distributed throughout the entire lung. With these improvements, we are beginning to capture images suggesting that MPs may accumulate in lung tissue, leading to phagocytosis by macrophages and infiltration of inflammatory cells into surrounding tissues.

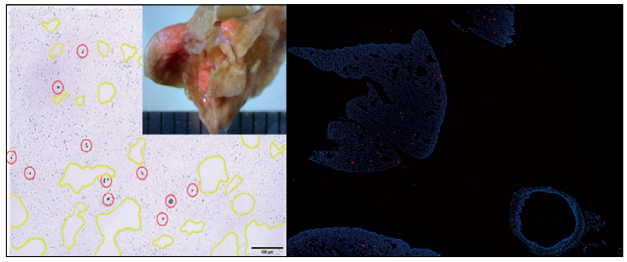

Bright-Field Image　　Fluorescence Microscopy Image

Fig. 3 Distribution and Accumulation of 3-μm Fluorescent Polystyrene Particles in Mouse Lungs Following Intratracheal Administration

(3) Establishment of a New Imaging Method

To analyze the behavior of MPs in biological tissues in greater detail and more efficiently, we have developed a new analytical workflow through a joint research project with Shimadzu Corporation. This innovative approach combines rapid screening with laser microscopy and precise identification by infrared Raman microscopy.

- **Large-Area Screening Using a 3D Measuring Laser Microscope (OLS5100)**

Using conventional microscopy and FTIR imaging, locating micrometer-scale particles within large tissue sections is extremely difficult and highly inefficient. The OLS5100 system employs a 405 nm short-wavelength laser and can acquire wide-area color images together with three-dimensional surface information at submicron resolution.

In our collaborative studies, unstained lung sections from MP-exposed mice were scanned over large areas using the OLS5100. As a result, we were able to rapidly identify particles exhibiting spherical morphologies and characteristic laser reflectance patterns that were distinct from those of surrounding biological tissue, even in low-magnification, wide-field images. This screening process has been shown to narrow the target locations (coordinates) for analysis, thereby dramatically reducing analysis time.

- **Definitive Identification Using an Infrared Raman Microscope (AIRsight)**

Point analyses are performed on the coordinates identified by the OLS5100 using an infrared Raman microscope (AIRsight). By analyzing the molecular vibration patterns specific to each substance, AIRsight can clearly distinguish whether a particle is polystyrene or a biologically derived protein or lipid. For example, when Raman spectra were obtained from spherical particles approximately 3 μm in diameter identified by the OLS5100, characteristic polystyrene peaks—including the benzene ring breathing mode near 1001 cm^{-1}—were clearly detected. These signals could be readily distinguished from those of the surrounding lung tissue, which exhibited protein-derived spectral peaks.

This combination of broad-area scanning and localized identification not only dramatically improves the efficiency of detecting minute MPs but also enables the acquisition of highly reliable data—free of false positives—by gathering evidence from both morphological (3D) and chemical (spectral) information. As such, it has the potential to become a powerful standard methodology for large-scale clinical analyses of MPs in biological specimens.

5. Future Research Directions and Challenges

Our studies to date have confirmed that MPs are physically present and persist in lung tissue in both humans and mice. We have also demonstrated that specialized techniques, such as the use of frozen tissue sections, are required for these observations. The research is now moving beyond simply confirming the presence of MPs to understanding the consequences. Our future research will focus on three primary objectives.

(1) Identification of Disease-Exacerbating Effects Using Mouse Disease Models

In addition to administering MPs to healthy mice, we will conduct experiments involving the intratracheal administration of environmentally relevant particle concentrations to mice with established disease models, such as chronic obstructive pulmonary disease (COPD), pulmonary fibrosis (bleomycin-induced), and bronchial asthma (ovalbumin-induced). Preliminary findings, including Masson's trichrome and collagen-I staining, suggest increased fibrosis in MP-exposed animals. Future studies will quantitatively and statistically evaluate how particle size (nanoplastics versus microplastics) and polymer type influence the production of inflammatory cytokines (such as IL-1β and TNF-α), as well as the expression of fibrosis markers (including α-SMA and Col-1). In addition, we will identify the risks associated with exposure to MPs, not only from their effects alone but also when combined with smoking and exposure to allergens.

(2) Elucidation of Molecular Mechanisms

To determine which signaling pathways are activated after MPs are taken up by lung epithelial cells and macrophages, we will conduct comprehensive gene expression analyses using RNA sequencing. Our preliminary findings suggest that MP exposure alters pathways involved in inflammation and cell death. In particular, we will focus on gene clusters involved in oxidative stress responses, cellular aging, and impaired tissue repair to identify the molecular mechanisms by which MPs trigger chronic inflammation and carcinogenesis.

(3) Expansion of Clinical Sample Analysis and Database Development

Leveraging the extensive clinical sample resources available at Nagasaki University Hospital (including lung cancer resection samples and bronchoalveolar lavage fluid (BAL) samples), we plan to conduct a large-scale investigation of MP accumulation in human lungs. Using the high-speed screening technology developed in collaboration with Shimadzu Corporation, we will examine associations between pulmonary MP burden and clinical factors, including residential environment (urban vs. rural), occupational history, and smoking history. A particular focus will be on determining whether MPs preferentially accumulate in tissue adjacent to lung tumors. This question is of considerable importance for assessing potential cancer-related risks and will be a major focus of future studies.

6. Conclusion

Microplastic pollution is no longer solely an environmental issue affecting the oceans. It has emerged as a significant concern with potential implications for respiratory health. Through proprietary techniques for preserving MPs in frozen tissue sections, a robust intratracheal administration model, and an integrated laser-Raman analytical platform developed in collaboration with Shimadzu Corporation, the Nagasaki University team is working, ahead of the rest of the world, to clarify the pathophysiological significance of MPs in the lung.

Our objective is to move beyond detection and uncover the fundamental functional and structural damage that MPs may cause at the cellular and tissue levels. Based on these findings, we aim to contribute to the development of guidelines for preventing health hazards associated with plastic pollution and to the creation of new treatment strategies. This is our ultimate goal. By integrating environmental science, medicine, and engineering, this project represents a highly significant challenge from the perspective of the SDGs, with considerable scientific and societal value.

Reference

[1] Tokito T, Kido T, Nagafuchi, et al. Microplastics in Human Bronchoalveolar Lavage Fluid. Respirology, 30:1141-1152, 2025.

Particle Analysis Using Infrared and Infrared-Raman Spectroscopy

Spectroscopy Business Unit, Analytical & Measuring Instruments Division
Naoya Fujiwara

1. Introduction

Microplastics are plastic particles with diameters of 5 mm or less, generated through the physical, chemical, and biological breakdown of larger plastic materials. Because living organisms can ingest these particles and accumulate them in their bodies, the potential impact on entire ecosystems has become of significant concern, prompting extensive research. A key aspect of microplastic research is understanding their distribution in the environment, which requires accurate analysis of plastic particles. In August 2025, Shimadzu Corporation released particle analysis and high-speed mapping software* packages as options for infrared and infrared Raman analysis, designed to streamline microplastic analysis.

This article describes the particle analysis and high-speed mapping functions provided by these software packages.

* The particle analysis and high-speed mapping software packages are available for AMsolution. AMsolution controls the AIMsight and AIM-9000 infrared microscopes, as well as the AIRsight infrared Raman microscope, and analyzes the data.

2. Particle Analysis Function

(1) What Is the Particle Analysis Function?

When analyzing microplastics collected from river or seawater samples, a typical procedure is to filter a known volume of water and then analyze the filter containing the captured particles using an infrared microscope or similar instrument. The analysis involves identifying particle components, calculating particle sizes, and analyzing statistical data.

The particle analysis function automatically detects particles in mapping data acquired with AMsolution according to a predefined component list and calculates characteristic parameters for each detected particle. The calculated parameters include major axis length, minor axis length, maximum Feret diameter, minimum Feret diameter, area, mass*, and volume*. The resulting data are processed statistically and displayed as bar charts, histograms, and other graphical outputs.

In addition to microplastic analysis, the function can be applied to contaminant analysis by selecting a different component list.

Section 2-(2) describes the workflow for the particle analysis function.

* Mass and volume are calculated using the theoretical equation reported in the reference paper below (Equation (1): log10 (M) = b·log10 (S) + a). This equation applies only to microplastics.
Shimadzu does not guarantee the validity or accuracy of the calculated mass values.

Tomoya Kataoka, Yota Iga, Rifqi Ahmad Baihaqi, et al. Geometric relationship between the projected surface area and mass of a plastic particle. Water Research. 2024;261:122061.

Mass and volume information for particles is considered useful when evaluating potential toxicological effects.

(2) Operating Procedure for the Particle Analysis Function

The particle analysis function supports both infrared and Raman mapping data. When infrared or Raman mapping data are loaded into the AMsolution analysis software, the Particle Analysis tab appears. Clicking this tab opens the particle analysis window (Fig. 1).

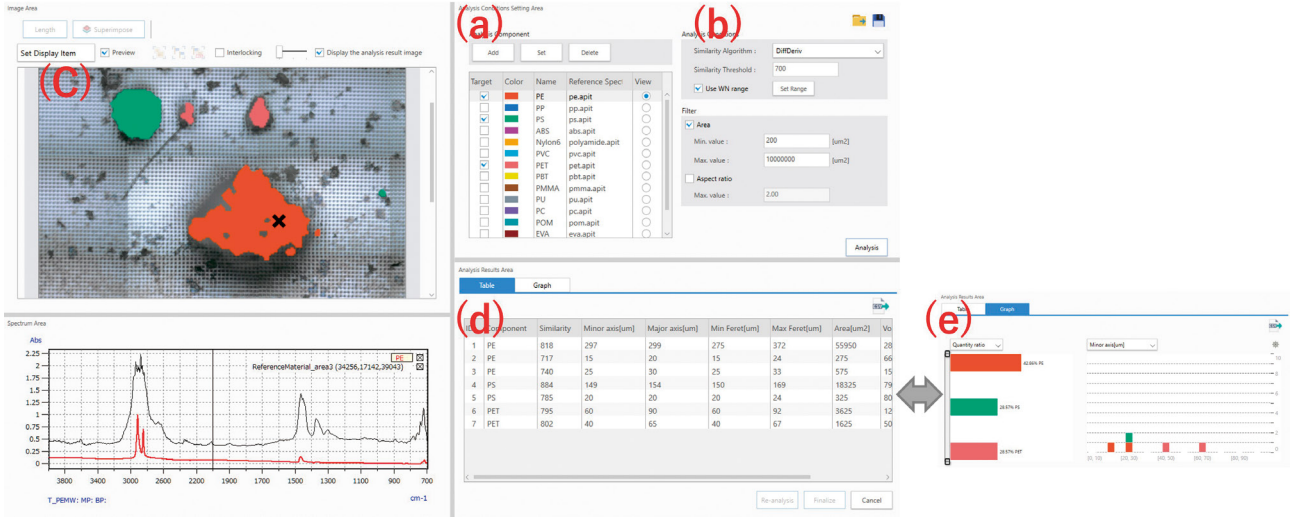

Fig. 1 Particle Analysis Window

The particle analysis function detects particles by calculating spectral similarity to reference spectra. Therefore, reference spectra must be registered before analysis. Register the reference spectra for the target components in the component list shown in Fig. 1 (a). Preset parameters are also available for microplastic analysis and contaminant analysis.

Once the reference spectra registration is complete, configure the analysis parameters as shown in Fig. 1 (b). The analysis parameters consist of three elements: algorithm type, threshold, and analysis wavenumber range. The analysis wavenumber range is shown in Fig. 2. The spectrum shown in Fig. 2 was acquired from microplastics collected on a PTFE filter. The yellow highlighted region indicates residual peaks originating from the filter. Because such peaks can adversely affect the analysis results, excluding the corresponding spectral region can improve identification accuracy.

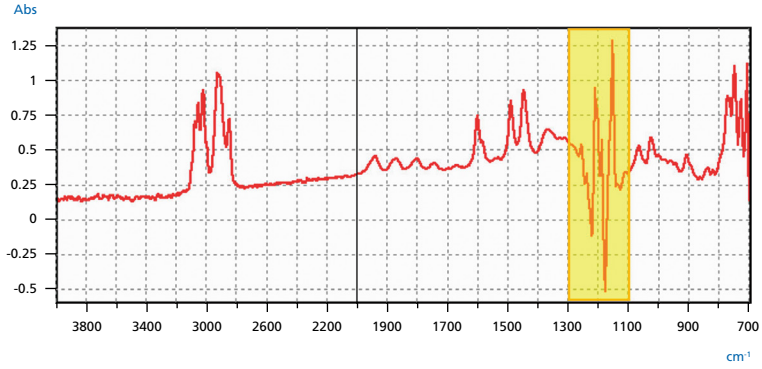

Fig. 2 Spectrum of Microplastics Collected on a PTFE Filter

After the reference spectra and analysis parameters have been configured, click the Analyze button to start the analysis. Once processing is complete, the detected particles are displayed in Fig. 1 (c). In addition, the characteristic parameters of the detected particles are calculated and displayed in the analysis results area (Fig. 1 (d)). The calculated parameters include major axis length, minor axis length, maximum Feret diameter, minimum Feret diameter, area, mass, and volume. Statistical analysis results can be viewed by selecting the Graph tab in the analysis results area (refer to Fig. 1 (e)).

Particle analysis results can be saved to a file and exported as reports or CSV files.

3. High-Speed Mapping Function

(1) What Is the High-Speed Mapping Function?

When measuring microplastics collected on a filter, the particles of interest are typically scattered across the filter surface. As a result, many measurement points correspond only to background regions with no target particles present (refer to Fig. 3). If background regions are measured using the same number of accumulations as regions containing particles, mapping measurements can require substantial acquisition time. To address this issue, the high-speed mapping function analyzes the spectrum acquired during the first accumulation and determines whether the measurement point corresponds to a background region or a region of interest (refer to Fig. 4). If the point is identified as a background region, measurement immediately proceeds to the next point, reducing overall acquisition time. For sample regions, measurements continue using the specified number of accumulations, preserving spectral quality in areas of interest.

Section 3-(2) describes the workflow for the high-speed mapping function.

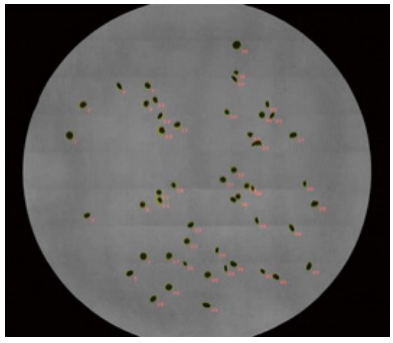

Fig. 3 Microplastics Collected on a Filter

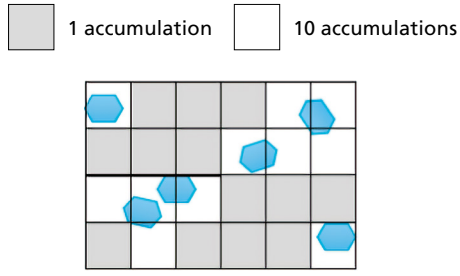

Fig. 4 Illustration of High-Speed Mapping (Example with 10 Accumulations)

(2) Operating Procedure for the High-Speed Mapping Function

To perform high-speed mapping, select the Execute High-Speed Mapping checkbox located above the Measure button (refer to Fig. 5). All other operations, including measurement-point registration, are identical to those used for standard mapping measurements.

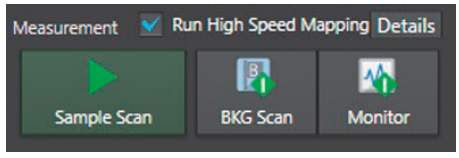

Fig. 5 High-Speed Mapping Checkbox

Once the checkbox is selected, the Details button becomes active. Clicking Details opens the high-speed mapping settings window (Fig. 6), where the required parameters are configured. The parameters required for high-speed mapping are the noise level, threshold, and exclusion wavenumber ranges. In high-speed mapping, peak detection is used to determine whether an area is part of the background.

The peak detection algorithm is the same as the one already built into the analysis software.

To obtain information useful for setting the parameters, take point measurements at representative points in the region of interest and the background region, and then compare the acquired spectra.

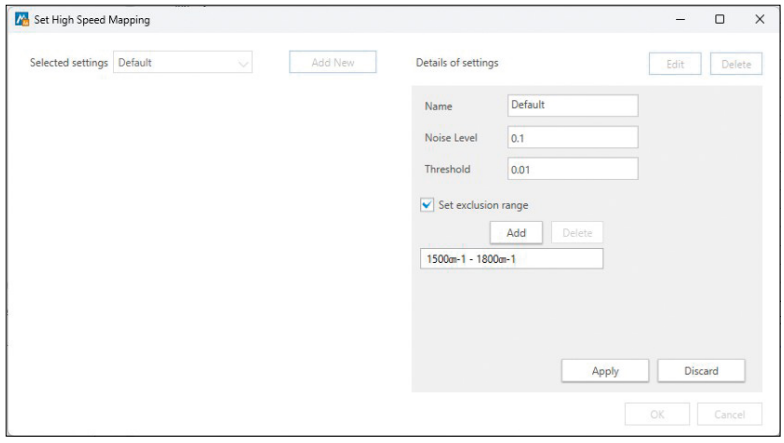

Fig. 6 High-Speed Mapping Details Setting Window

After configuring the parameters, click OK to close the setting window, then click the Measure button to start the measurement.

Regions identified as background can be reviewed in the analysis software. When the spectrum at a measurement point is displayed on a graph, the spectrum name appears in the legend. Spectra whose names begin with "SKIP_" indicate measurement points that were identified as background regions.

4. Conclusion

This article introduced the particle analysis function, which can be used for microplastic and contaminant analysis, and the high-speed mapping function, which enables faster measurements while maintaining spectral quality. We also encourage you to access our Application News bulletins [1], [2] that feature examples of utilizing the particle analysis function and high-speed mapping.

References

[1] Kazuki Sobue, "High-Speed Measurement of Microplastics Smaller than 100 µm Collected on a Filter and Efficient Analysis—Using a High-Speed Mapping Program and Particle Analysis Program—," Shimadzu Application News 01-00994

[2] Yoshiyuki Tange, "Analyzing Microscopic Contaminants Embedded in Recycled Plastic," Shimadzu Application News 01-01001

Notes on Infrared Spectral Analysis – Amides –

Solutions COE, Analytical & Measuring Instruments Division
Yoshiyuki Tange

1. Introduction

In the previous issue (FTIR TALK LETTER Vol. 45), we explained how carbonyl compounds can be classified using infrared absorption peaks other than the C=O stretching vibration. As an example of an application, we also introduced the infrared spectrum of FAME (fatty acid methyl esters). In this issue, we discuss the classification of amides and present practical methods for identifying nylon materials.

2. Classification of Amides

An amide group is a functional group consisting of an amino group (-NH_2) bonded to a carbonyl group (C=O). Accordingly, amide compounds can be readily identified in infrared spectra by the presence of N-H stretching bands at 3350-3100 cm^{-1}, the Amide I band near 1650 cm^{-1}, arising from C=O stretching, and the Amide II peak at slightly lower wavenumbers arising from a combination of N-H bending and C-N stretching vibrations (Fig. 1). Other characteristic amide absorptions include: Amide III near 1260 cm^{-1} and Amide IV near 940 cm^{-1} [1].

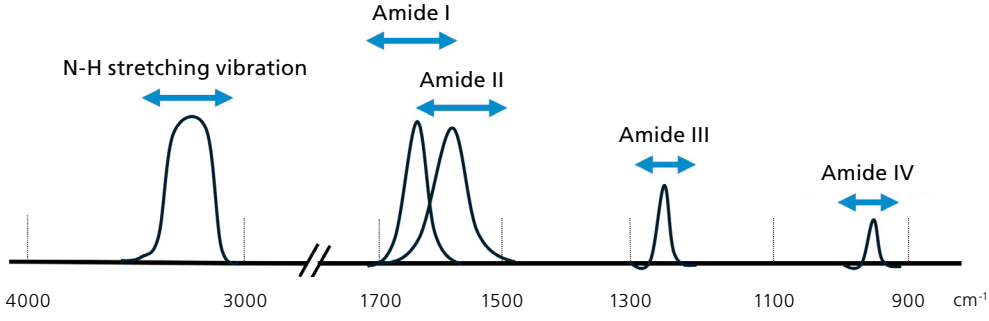

Fig. 1 Major Infrared Absorption Peaks Associated with Amide Groups

Fig. 2 shows the position of key peaks in the infrared spectrum of a compound with amide groups and how to classify those peaks. Amides are classified as primary, secondary, or tertiary according to the number of hydrogen atoms attached to the nitrogen atom. Differences among these classes are reflected in the 3350-3100 cm^{-1} peak region and in the Amide I and Amide II peaks.

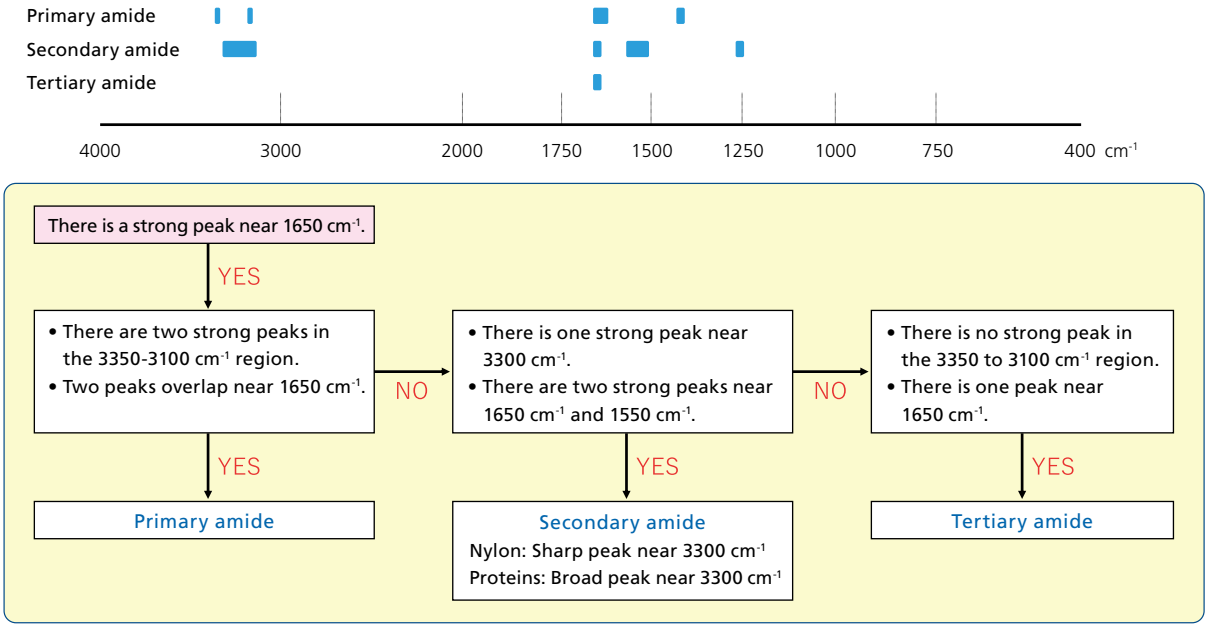

Fig. 2 Position of Key Peaks in the Infrared Spectrum of a Compound with Amide Groups and How to Classify Those Peaks

(1) Distinguishing Primary, Secondary, and Tertiary Amides

Fig. 3 shows the infrared spectrum of butyramide, a primary amide, together with assignments of the major absorption peaks. Primary amides contain two hydrogen atoms attached to the nitrogen atom. Consequently, two N-H stretching bands are observed, producing absorption peaks near 3350 cm^{-1} and 3200 cm^{-1}. In addition, the Amide II band, arising from NH_2 bending vibrations, overlaps with the Amide I band around 1600 cm^{-1}.

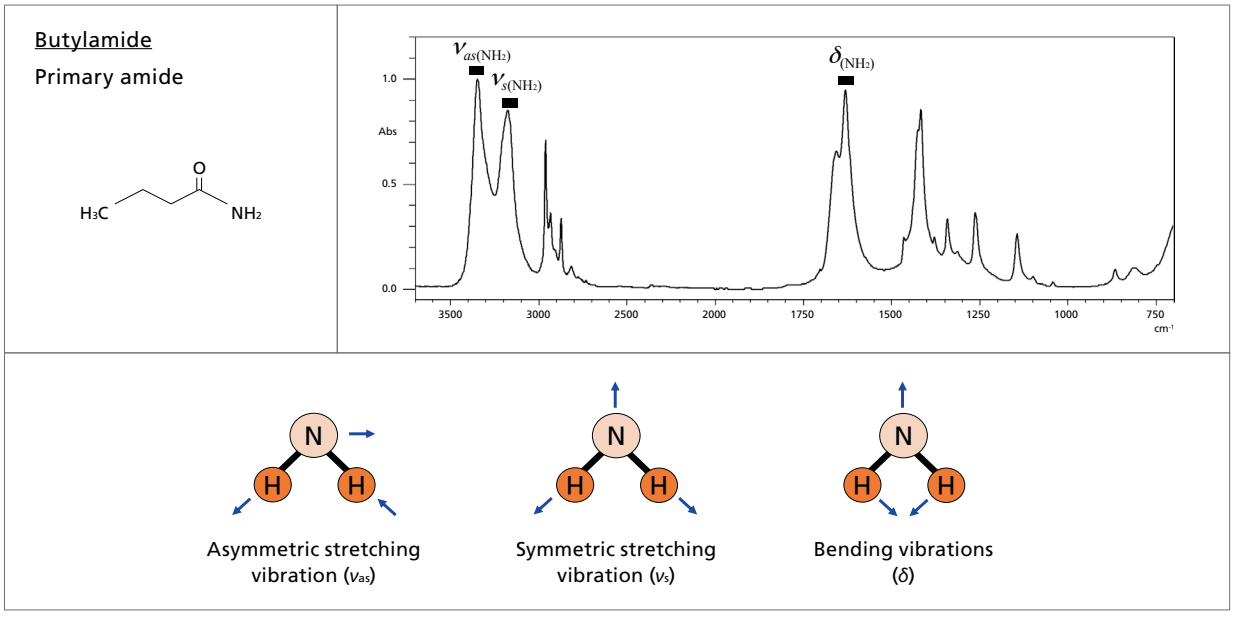

Fig. 3 Infrared Spectrum of Butyramide

Secondary amides contain only one hydrogen atom attached to the nitrogen atom. Accordingly, a single N-H stretching peak appears near 3300 cm^{-1}. In addition, Amide II is separated from Amide I due to the mixing of the C-N stretching vibration with the N-H bending vibration of the C-N-H group, and a peak appears around 1550 cm^{-1}.

Fig. 4 shows the infrared spectrum of N,N'-ethylenebisstearamide, a secondary amide, together with assignments of the N-H-related bands.

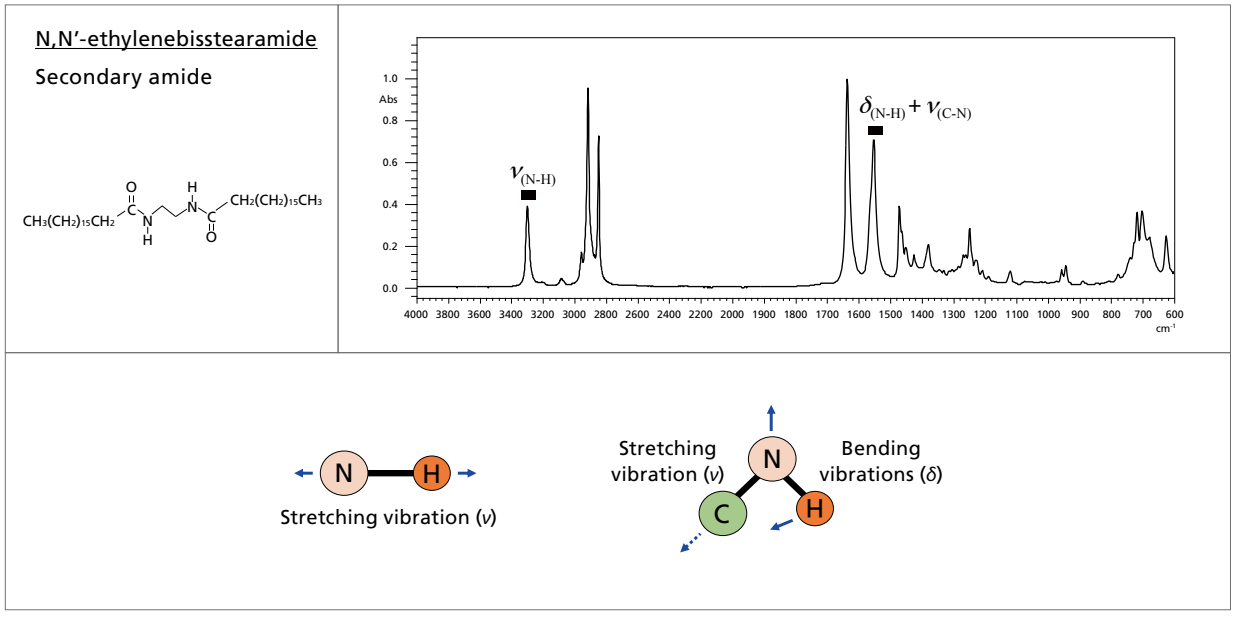

Fig. 4 Infrared Spectrum of Polyamide and Assignment of Peaks Attributable to N-H Groups

Fig. 5 shows the infrared spectrum of dimethylformamide, a tertiary amide. Because tertiary amides contain no N-H groups, no peak is observed in the 3350-3100 cm^{-1} region. Furthermore, the Amide II peak is absent. As a result, only one peak appears near 1650 cm^{-1}, corresponding to Amide I.

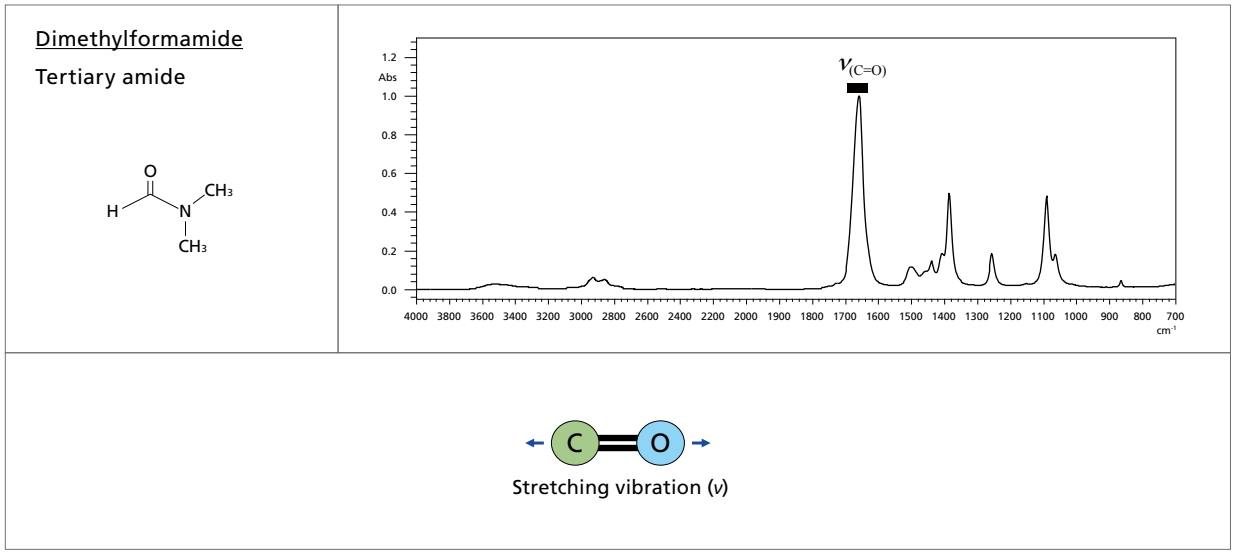

Fig. 5 Infrared Spectrum of Dimethylformamide and Assignment of the Peaks Derived from the C=O Group

(2) Identifying Proteins

Fig. 6 shows the infrared spectrum of human hair as an example of a protein. Hair consists primarily of keratin, a protein composed of 18 amino acids. Since proteins are formed when amino acids form peptide bonds, with the carboxyl group (-COOH) and the amino group (-NH_2) forming an amide group, they can be considered a type of secondary amide. The infrared spectrum of hair reveals a single peak attributed to the N-H stretching vibration around 3300 cm^{-1}, which is characteristic of secondary amides, as well as peaks in the Amide I and Amide II absorption bands. In addition, since proteins contain water, characteristic peaks derived from OH groups are observed. If the peak around 3300 cm^{-1} is a broad peak resulting from the overlap of the N-H stretching absorption derived from the amide group and the OH stretching absorption, the substance can be identified as a protein.

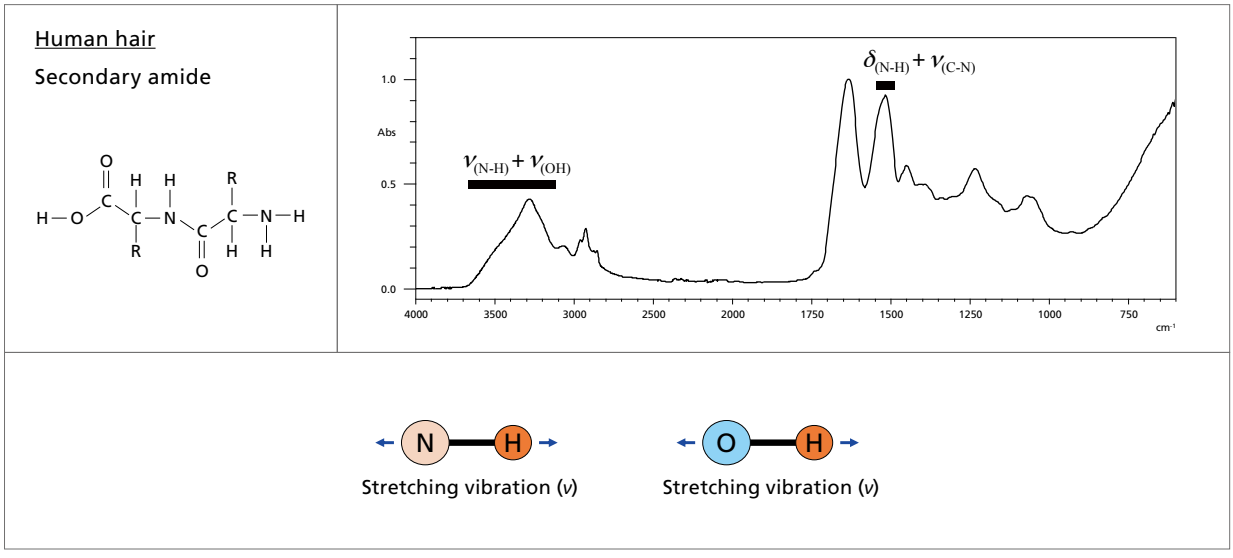

Fig. 6 Infrared Spectrum of a Protein and Vibrational Modes Responsible for the Peak Near 3300 cm^{-1}

3. Identification of Nylon

Nylon, a type of polyamide, is widely used because of its high strength, heat resistance, and chemical resistance. Although "Nylon" was originally a trademark of DuPont, the company that first developed polyamide 66 as a synthetic fiber, it has since become a generic name. There are many types of nylon, each with different physical properties, such as melting point and water absorption (Table 1). Because their molecular structures differ slightly, FTIR is sometimes used to quickly identify different types of nylon.

Table 1 Representative Types of Nylon and Their Properties [2]

Type	Density (g/cm^3)	Melting Point (°C)	Absorption (%)
Nylon 6	1.14	215-225	1.3-1.9
Nylon 66	1.14	255-265	1.1-1.5
Nylon 11	1.04-1.05	184-187	0.3
Nylon 12	1.01-1.02	176-180	0.25

(1) Spectral Characteristics of Different Nylon Types

All nylon materials exhibit the characteristic infrared spectral features of secondary amides shown in Fig. 7. The number to the right of the name indicates the number of carbon atoms between the amide groups. While Nylon 11 is produced from bio-based feedstock and Nylon 12 is produced from petroleum-derived feedstock, both contain relatively high proportions of CH groups relative to amide groups. In the infrared spectrum, Nylon 11 and Nylon 12 exhibit a strong peak around 2800 cm^{-1}—the absorption band corresponding to the CH group—making them easily distinguishable from Nylon 6 and Nylon 66.

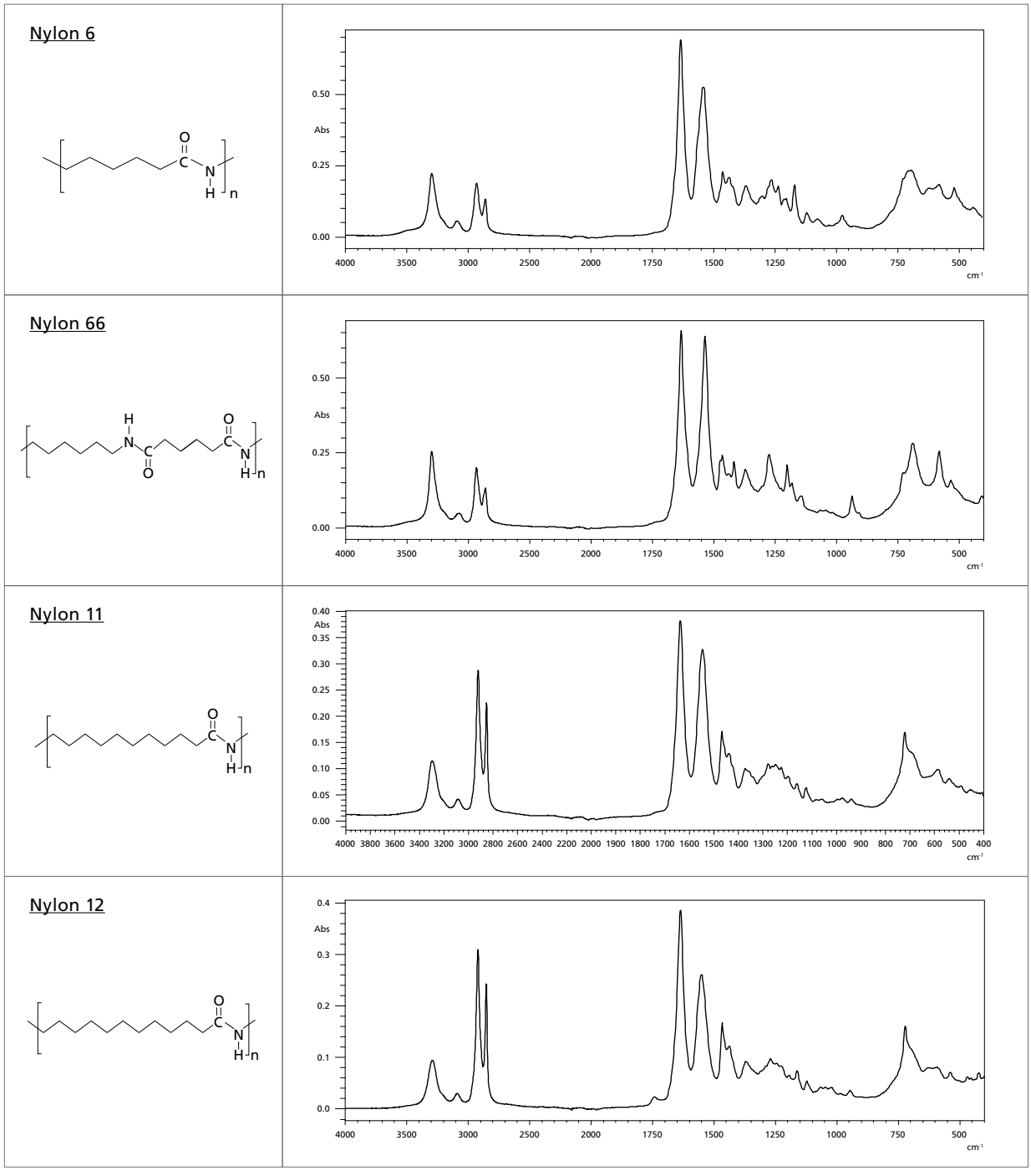

Fig. 7 Infrared Spectra of Typical Nylon Materials

(2) Distinguishing Nylon 6 from Nylon 66

Fig. 8 shows the infrared spectra of Nylon 6 and Nylon 66 in the 850-1050 cm^{-1} region, along with their respective crystal structures. These materials can be differentiated based on differences in their crystal structures. The crystal structures of Nylon 6 are primarily of the α-type and γ-type. The α-type has an anti-parallel crystal structure, in which the main chains run in opposite directions. This allows hydrogen bonding to occur at all amide groups when the molecular chains are in an extended conformation. On the other hand, the γ-type adopts a parallel crystal structure in which the main chains run in the same direction, resulting in a twisted structure that allows hydrogen bonding between the amide groups. Peaks attributable to the α-type crystal structure appear at 960 cm^{-1} and 930 cm^{-1}, while those attributable to the γ-type appear at 973 cm^{-1} [3]. The infrared spectrum shown in Fig. 8 exhibits strong peaks attributable to the γ-type crystal structure, indicating that the γ-type is the dominant crystal structure. In contrast, Nylon 66 has a crystal structure in which the molecular chains are arranged in an orderly fashion, and it can be identified by the 936 cm^{-1} peak attributed to the C-C bonds in the trans conformation of the crystalline phase [4].

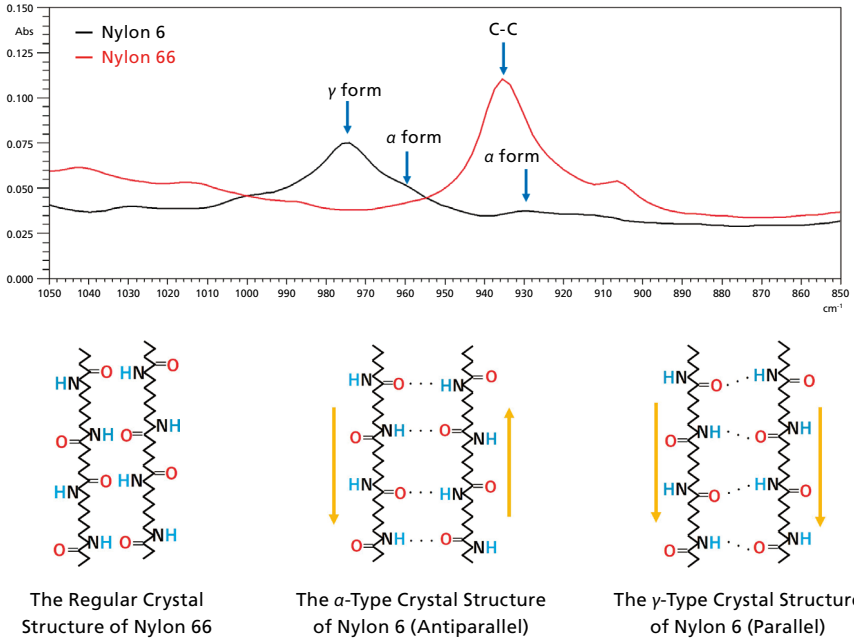

The Regular Crystal Structure of Nylon 66

The α-Type Crystal Structure of Nylon 6 (Antiparallel)

The γ-Type Crystal Structure of Nylon 6 (Parallel)

Fig. 8 Infrared Spectra of Nylon 6 and Nylon 66 in the 1050-850 cm^{-1} Region and their Crystal Structures

4. Conclusion

This article explained how amides can be classified.

- By focusing on the peaks around 3350-3100 cm^{-1} and 1650 cm^{-1}, it is possible to classify primary, secondary, and tertiary amides.
- Among secondary amides, proteins can be identified by examining the shape of the peak at 3300 cm^{-1}.
- Nylon 11, Nylon 12, Nylon 6, and Nylon 66 can be distinguished by the intensity of the peak around 2800 cm^{-1}.
- Nylon 6 and Nylon 66 can be distinguished by differences in the peaks between 1000 and 900 cm^{-1} that result from their crystal structures.

Next time, we will discuss amines—which, like amides, contain amino groups—and introduce methods for analyzing their infrared spectra.

References

[1] C. Zhou et al., Polymer 190, 122231 (2020).

[2] The Japan Society for Analytical Chemistry, Polymer Analysis Handbook, KINOKUNIYA COMPANY, LTD. (2020)

[3] N. Vasanthan and D. R. Salem, J. polym. sci., B, Polym. phys. 39, 536 (2001)

[4] N. Vasanthan and D. R. Salem, J. polym. sci., B, Polym. phys. 38, 516 (1999)

IR 70th ANNIVERSARY

1956 — AR-275

Double beam, self-recording infrared spectrophotometer.

1965 — IR-27G

Double beam, self-recording infrared spectrophotometer equipped with a grating, significantly improving maintainability.

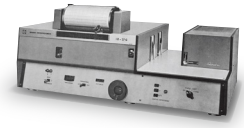

1981 — IR-435

Double beam, self-recording infrared spectrophotometer equipped with a built-in data processor and parallel printer.

1984 — FTIR-4000

A Fourier transform infrared spectrophotometer that greatly improved light efficiency compared to the split-type model.

1990 — FTIR-8100

Reduced both size and cost, while also providing multi-functional, high-end performance.

2002 — IRPrestige-21

High-end FTIR equipped with a newly developed interferometer, achieving the industry's highest S/N ratio of 40,000:1.

2008 — IRAffinity-1

Reduced size by 20 % compared to conventional models. Equipped with a new foreign particle analysis program.

2013 — IRTracer-100

Achieved high performance with a S/N ratio of 60,000:1 and resolution of 0.25 cm^{-1}.

2017 — IRSpirit

A compact, high-performance FTIR with an A3-size footprint and a weight of 8.5 kg.

2022 — IRXross

Achieved S/N comparable to high-end instruments while maintaining a mid-class size.

2022 — AIRsight

Unique instrument combining infrared and Raman microscopes, enabling one-stop infrared and Raman analysis.

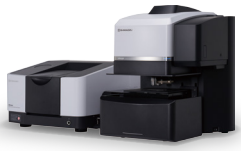

2023 — AIMsight

Equipped with a wide-field camera, enabling an easy "Observe > Measure > Analyze" infrared analysis process.

2023 — IRSpirit-X

A compact, high-performance FTIR designed for both simple operation and reliability, backed by a 10-year warranty.

2026

SHIMADZU

Shimadzu Corporation

www.shimadzu.com/an/